Mode Coupling Analysis of Interfacial Stability and Critical Anode–Cathode Distance in a 500-kA Aluminum Electrolysis Cell

MAO LI,[1] SUYU MA,[1] HESONG LI,[1] WENYUAN HOU ⓘ,[1,2]
BENJUN CHENG,[1,3] TING HU,[1] and YUJIE WANG[1]

1.—School of Energy Science and Engineering, Central South University, Changsha 410083, China.
2.—e-mail: zndxhwy@163.com. 3.—e-mail: Chbj666@mail.csu.edu.cn

The quantitative description and theoretical research on the stability of the electromagnetic field interfacial wave in aluminum electrolysis cells are the key to achieving high energy efficiency and operational safety. The magneto-hydrodynamics equations were established based on the theory of electromagnetics and hydrodynamics and applied to a 500-kA cell. The Fourier series expansion and finite element methods were used for modeling and simulation of interfacial stability. Detailed analysis was conducted on wave mode coupling regimes by custom code in MATLAB. Based on the characteristics of total modulus, a modal analysis method was proposed to clarify how anode–cathode distance (ACD) and length-width ratio of cells affected interfacial stability. The results indicate that the stability is enhanced as the increase of ACD for a 500-kA electrolysis cell and the critical ACD is derived as 0.041 m, which is preferable for stabilizing the cell and reducing energy consumption.

INTRODUCTION

With the development of large-scale cell capacity, the horizontal current with a magnetic background field plays a decisive role in deciding cell stability and energy consumption. The potential safety hazards in industrial production have been exposed because of the interfacial wave instability, which is the limitation in the development of large-scale applications.[1–3] Hence, investigating the mechanism of magneto-hydrodynamics (MHD) stability and maintaining the electromagnetic field interfacial stability are of significant importance to the safety production of the large-scale cells.[4,5]

Intensive investigations and multiple mathematical models have been carried out to evaluate MHD stability during past decades. Sele[6] studied the transient waves on the metal surface and explained the mechanism of the rotating wave. Urata et al.[7,8] observed the two-liquid layer system and proposed "the MHD equations", one for magneto-interfacial wave motion containing an electromagnetic force

term and another for the distribution of electrical currents, and then found that the instability was governed by the distribution of the vertical component of the magnetic field. Sneyd et al.[9] showed that the instability can occur via mode interactions and similar frequencies, and two modes may become unstable. A criterion for instability was presented by Davidson et al.[10,11] A two-dimensional shallow-water equation was established to analyze the mechanisms of the instability in the cell. The coupling mechanism resulted in the instability of the magnetic fluid within a certain range. Several works had been devoted to the MHD stability models for three-dimensions.[12–15] They presented new expressions for quantities and assessed the impact of busbar configuration, current density, anode–cathode distance, and irregular cathode surfaces on the MHD stability.

The close coupling between two immiscible fluids and electromagnetic field also brings many challenges for numerical simulation. Bojarevics et al.[16–20] introduced a stability criterion with the use of perturbation techniques and the coupling mechanism for the horizontal motion of the magneto-fluid. It was the first attempt to apply the

distribution of friction resistance into the model. In addition, the numerical results for 500-kA cells were used to analyze the cell stability under a combination of the effects.[21,22] The linear model reflected the characteristics of interfacial stability to a certain extent based on reasonable assumptions. Sun et al.[23] established a non-linear coupling model and investigated the impact of the fluid flow rate on stability. Kadkhodabeigi et al.[24] added friction to the model in the form of a source term, and developed a nonlinear electromagnetic field wave equation based on assumptions. Molokov et al.[25–27] presented the classification of instability modes based on the asymptotic theory for high values of the ratio of Lorentz force and gravity, and then proposed obstacles to suppress the interfacial wave instability. Some studies referred to the operation process of simulation software to calculate MHD stability, which provided some methods for research. Ruan et al.[28] and Yang et al.[29] analyzed the MHD instability in reduction cells with the Lyapunov method, and observed that there were three types of status for fluid flow motion in reduction cells. Li et al.[30,31] developed a finite element model to examine the interfacial wave with a novel cathode structure and solved it by the Maxwell equations.

Reducing energy consumption is the priority in developing new technologies for the aluminum electrolysis industry. One important measurement technology is to reduce the anode–cathode distance (ACD), but this increases MHD instability and affects production instability. Tian et al.[32,33] proposed a "three-layer composition model" of ACD based on the structural aspect. Xu et al.[34] and Zhang et al.[35] established a nonlinear MHD shallow-water model and proposed a critical ACD based on the qualitative view of the interface deformation degree. Lu et al.[36] studied the effect of ACD on the thermo-electrical behavior by ANSYS. Hua et al.[37] presented a CFD-based multiphase MHD flow model and bath–metal interface deformation. Conceptually similar to aluminum electrolysis cells, MHD stability of bath–metal interfaces also appears in liquid–metal batteries.[38,39] A long-wave interface instability was studied by Weber et al.[40] and Horstmann et al.,[41] and a nonlinear shallow-water model was presented by Zikanov.[42] A wave coupling model for the analysis of interfacial waves was suggested by the studies of liquid–metal batteries.

According to the literature, a two-dimensional model used in the study of interfacial stability is an effective approximation. Although there are many studies on MHD stability for different kinds of models, the mechanism for describing the electromagnetic field interfacial wave based on the modal analysis is not clear. The critical ACD which can obtain excellent production targets under the production of low voltages has also rarely been studied. As far as we know, there is no published literature describing the interfacial stability based on a

quantitative analysis method or that has studied the critical ACD that takes into consideration the wave mode coupling in a 500-kA cell.

In this work, based on the electromagnetic calculations with ANSYS of a 500-kA cell, after fitting the magnetic field distribution at the magnetic fluid interface, the coupled interfacial wave equations were solved by the Fourier series method and the finite element method (FEM). The Fourier and energy spectrum representing the stability of interfacial wave were solved by custom code MATLAB, and the contributing modulus of the unstable component was calculated. A modal analysis method was proposed to quantitatively measure the stability of the interfacial wave. Detailed analysis was focused on a series of ACD which played an important role in the stability of electromagnetic field interfacial wave, and the ACD maintaining the stability of the interface, as well as reducing energy consumption, was derived. To verify the feasibility of the modal analysis method on other parameters, we used modal analysis on a series of length–width ratios (LWR) and compared the total modal to obtain the effect of LWR on the stability.

MODEL DESCRIPTION

Physical Model and Basic Assumptions

In the process of aluminum electrolysis, the melt flow is a typical multiphase flow, which consists of two fluids, the metal and the bath, as well as discrete anode bubble and alumina particle phases. In addition to gravity and the electromagnetic and viscous force, the melt in the cell may be affected by bubble forces and interphase forces. It would be very difficult and unachievable to incorporate each of these factors into the model. This paper focuses on the coupling among the electromagnetic field, flow field, and status of the fluid flow. According to Ref. 43, the results from two-dimensional and three-dimensional models were compared and they did not differ much. However, the computational volume of transient study using three-dimensional model is huge and it consumes a lot of resources. Thus, a two-dimensional model is an effective approximation to the object of study.

Several assumptions are made as follows:

1. The vertical flow is ignored and the horizontal velocity is only considered for the numerical analysis of MHD stability in a two-dimensional dynamic model.[8,44]
2. The phases of anode bubbles and alumina particles are ignored.
3. No temperature change effects on physical properties, which are stable in the electrolysis process, are taken into consideration. And there is no mass transfer between the metal and bath.

The shape of the aluminum electrolysis cell was geometrically simplified to a rectangular shape with

Mode Coupling Analysis of Interfacial Stability and Critical Anode–Cathode Distance in a 500-kA Aluminum Electrolysis Cell

2743

a horizontal length L_x of 19.24 m and width L_y of 3.58 m. The horizontal aluminum h_1 was 0.20 m and the anode–cathode distance h_2 was 0.04 m. Other production processes and material properties used in the computation of MHD were obtained from a 500-kA field cell, which are shown in Table S-I (refer to the online supplementary material).

Mathematical Model

The Navier–Stokes equation has been applied in the aluminum electrolysis, and the basic governing equations are:

$$\nabla \cdot U = 0 \tag{1}$$

$$\rho\left(\frac{\partial U}{\partial t} + U \cdot \nabla U\right) = -\nabla P + \mu\nabla^2 U + \rho g\nabla H + F \tag{2}$$

where U is the velocity of the fluid flow, P is the pressure, ρ is the density of the fluid, μ is the kinematic viscosity of the fluid flow, t is the time, g is acceleration of gravity, H is the height of bath–metal interface, and F is Lorentz factor.

All relevant physical quantities can be separated into stationary and non-stationary parts. The stationary part describes a stationary physical system. The addition of the non-stationary part of physical quantities is expressed as harmonic function about time, and the function is:

$$H = H_0 + h \cdot e^{i\omega t} \tag{3}$$

where P, U, and F can also be expressed as above. The non-stationary part has been substituted into Eqs. 1 and 2, and the divergence of the equation was taken. Based on the free boundary condition, the wave equation can be obtained as:

$$\left(\frac{\rho_1}{h_1} + \frac{\rho_2}{h_2}\right)\frac{\partial^2 \xi}{\partial t^2} - g\Delta\rho\nabla^2\xi = -\nabla(f^1 - f^2) \tag{4}$$

where ρ_1 and ρ_2 are the density of the metal and the bath, h_1 and h_2 are the depth of the metal layer and ACD, ξ is the disturbance wave height of metal surface, and f^1 and f^2 are the perturbing electromagnetic force of the metal and the bath, respectively.

The electromagnetic force in the metal layer is an important part of the perturbation, which is generated by the perturbed current density and magnetic flux density in the vertical direction B_z. The perturbing electromagnetic force f^2 in the bath layer is ignored. Equation 4 is simplified as:

$$\left(\frac{\rho_1}{h_1} + \frac{\rho_2}{h_2}\right)\frac{\partial^2 \xi}{\partial t^2} - g\Delta\rho\nabla^2\xi = \sigma_1\left(\frac{\partial\varphi}{\partial y}\frac{\partial B_z}{\partial x} - \frac{\partial\varphi}{\partial x}\frac{\partial B_z}{\partial y}\right) \tag{5}$$

where φ is the electrical potential, and σ_1 is the electrical conductivity of metal. The boundary conduction of the wave equation is:

$$g\Delta\rho\frac{\partial\xi}{\partial n} = \sigma_1 B_z\left(n_y\frac{\partial\varphi}{\partial x} - n_x\frac{\partial\varphi}{\partial y}\right) \tag{6}$$

Since the conductivity of the metal is much larger than that of the anode carbon, and the conductivity of the anode carbon is much larger than that of the bath, the potential equation proposed by Segatz et al.[43] can be simplified as:

$$h_1 h_2\nabla^2\varphi = -\frac{J_z}{\sigma_1}\xi \tag{7}$$

The boundary conduction of the potential equation is:

$$\frac{\partial\varphi}{\partial n} = 0 \tag{8}$$

where J_z is the vertical current in the bath. The flowchart shows the establishment of the mathematical model for the study, and is shown in supplementary Fig. S-1 (refer to the online supplementary material).

Numerical Methods

According to the mathematical model section, interfacial stability equations are partial differential equations. These are transformed into eigenvalues using FEM. Supplementary Fig. S-2 shows the schemes of the numerical methods. In response to the above proposed set of equations for stability, the Fourier series method has been used to expand the disturbance part of the physical quantity into the sum of a series of Fourier components according to the principle of numerical analysis. The Fourier component function is defined as:

$$\eta_{m,n} = \frac{2}{\sqrt{L_x L_y}}\varepsilon_{m,n}\cos\left(\frac{m\pi}{L_x}x\right)\cos\left(\frac{n\pi}{L_y}y\right) \tag{9}$$

where the basic function $\eta_{m,n}$ satisfies the normalized orthogonality in different modes. The expression used is shown in:

$$\varepsilon_{m,n} = \begin{cases} 1, & m,n \neq 0 \\ \frac{1}{\sqrt{2}}, & mn = 0, m \neq n \\ \frac{1}{2}, & m = n = 0 \end{cases} \tag{10}$$

The solutions to the equation of wave potential can be expressed as linear combinations of infinite series at different frequencies, as:

$$\xi(x,y,t) = \sum_{m,n}\xi_{m,n}\eta_{m,n}e^{i\omega t} \tag{11}$$

$$\varphi(x,y,t) = \sum_{m,n}\varphi_{m,n}\eta_{m,n}e^{i\omega t} \tag{12}$$

where $\xi_{m,n}$ and $\varphi_{m,n}$ are the mode components (m,n) of the wave height ξ and potential φ at frequency ω, respectively.

Derived from Eqs. 7, 8 and 11, 12, the potential equation which represents the wave height of the metal can be obtained in Eq. 13:

$$\varphi = \beta \sum_{m,n} \frac{1}{\Delta_{m,n}} \xi_{m,n} \eta_{m,n} e^{i\omega t} \qquad (13)$$

where $\beta = \frac{J_z}{\sigma_1 h_1 h_2}$ and $\Delta_{m,n} = \left(\frac{m\pi}{L_x}\right)^2 + \left(\frac{n\pi}{L_y}\right)^2$.

According to Gauss–Green's Theorem and Eqs. 5 and 9, the matrix equation for eigen-values is shown below:

$$\left[\left(\frac{\rho_1}{h_1} + \frac{\rho_2}{h_2}\right)\omega^2 - g\Delta\rho\Delta_{m,n}\right]\xi_{m,n}$$
$$- \sigma_1\beta \sum_{m',n'} S_{(m,n)(m',n')}\left(1/\Delta_{m',n'}\right)\xi_{m',n'} = 0 \qquad (14)$$

where

$$S_{(m,n)(m',n')} = \left\langle \frac{\partial\eta_{m,n}}{\partial x}, B_z \frac{\partial\eta_{m',n'}}{\partial y}\right\rangle - \left\langle \frac{\partial\eta_{m,n}}{\partial y}, B_z \frac{\partial\eta_{m',n'}}{\partial x}\right\rangle.$$

The value of the matrix S indicates:

1. The coupling between two modes becomes strong, then eigenvalues will be complex and waves will fluctuate exponentially and become unstable.
2. The matrix S is an antisymmetric.[44]
3. No coupling between longitudinal modes nor between two horizontal modes.
4. The degree of mode coupling is significantly influenced by the vertical magnetic.

By solving Eq. 14, the eigen-frequency ω of MHD is obtained to determine the stability in the aluminum electrolysis cell, and is generally in the plural form, $\omega = \omega_r + i\omega_s$, with its real component ω_r representing the fluctuation frequency and the imaginary part ω_s representing the fluctuation growth rate. The fluctuation of the bath–metal interface decreases with time at $\omega_s > 0$ and increases at $\omega_s < 0$.

Fitting of Vertical Magnetic Field

The magnetic induction of the vertical magnetic field in metal is the key to electromagnetic disturbance. The least absolute residuals method based on the custom code in MATLAB has been used to fit the vertical magnetic field. Through the comparison of SSR, R-square, Adjusted R-square, RMSE, and other indicators, the strength of fitting the magnetic induction in a vertical magnetic field can be defined as:

$$B_z = \sum_{p=5}\sum_{q=4} a_{pq} x^p y^q \qquad (15)$$

where the value a_{pq} of the parameters used in the fitting function are shown in supplementary Table S-II.

RESULTS AND DISCUSSION

MHD Stability Analysis

According to the vertical magnetic field surface fitting method, the discrete data of the vertical magnetic field in a 500-kA aluminum electrolysis cell is fitted by custom code in MATLAB. The distribution of the steady-state vertical magnetic field components is shown in Fig. 1.

Applying the relevant parameters and the surface fitting values of the vertical magnetic field in the 500-kA large aluminum electrolysis cell into Eq. 14, the characteristic matrix S can be obtained and is listed in supplementary Table S-III.

According to Table S-III, for a 500-kA large aluminum electrolysis cell, the corresponding value of the modes (1, 2) and (3, 0) is the largest in the matrix S. Thus, the degree of coupling between these two modes is strongest, which is susceptible to MHD instability. Through substituting the values of the characteristic matrix S obtained above and the relevant parameters of the 500-kA large aluminum electrolysis cell into Eq. 14, the Fourier and the intensity spectrum of the cell are solved by custom code in MATLAB and the results are shown in Fig. 2.

Figure 2 demonstrates the growth rate and the energy intensity of the unstable components. The counts of the peaks represent the number of unstable frequencies in the MHD system. The number of unstable frequencies in a 500-kA aluminum electrolysis cell is four, as observed in Fig. 2. They represent the degree of instability at that frequency. Among them, the fourth component from left to right, with the largest energy intensity and the largest growth rate, is most likely to cause the instability. A portion of the obtained eigen-frequency contains imaginary parts, indicating that the MHD system oscillates unsteadily.

It can be seen that the instability components are mainly concentrated in the lower frequency region (0.05–0.30 Hz), in which are the characteristic frequencies of the unstable component with the largest growth rate and energy intensity, that is 0.3001–0.2866i, with the perturbing frequency of 0.3001 and a period of 21 s. The periods of modes are 30 s and 23 s, respectively, and they are in good agreement with the experiment results of typically 20–40 s.[44] The main moduli of the eigen-frequency of 0.3001–0.2866i are listed in Table I.

It can be concluded from Table I that the unstable component is formed by the combined action of several modes, in which the mechanisms of mutual excitation, such as (1, 1) and (0, 2), are the most prominent, accounting for about 70% of the total. Similarly, the mechanisms of mutual excitation of the other unstable components can be obtained. The coupling relationships and effects of each mode are different for various unstable components.
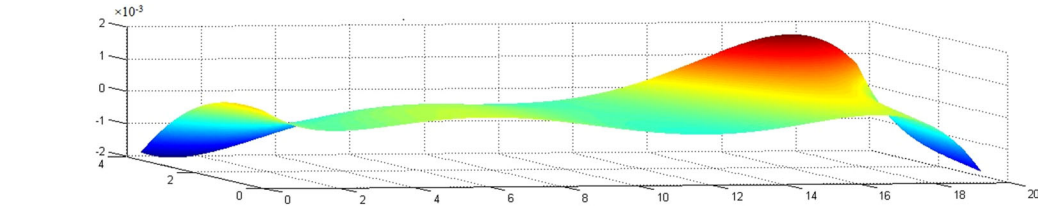
Mode Coupling Analysis of Interfacial Stability and Critical Anode–Cathode Distance in a 500-kA Aluminum Electrolysis Cell

2745

Fig. 1. The distribution of B_z for the 500-kA cell.

(a) the frequency spectrum
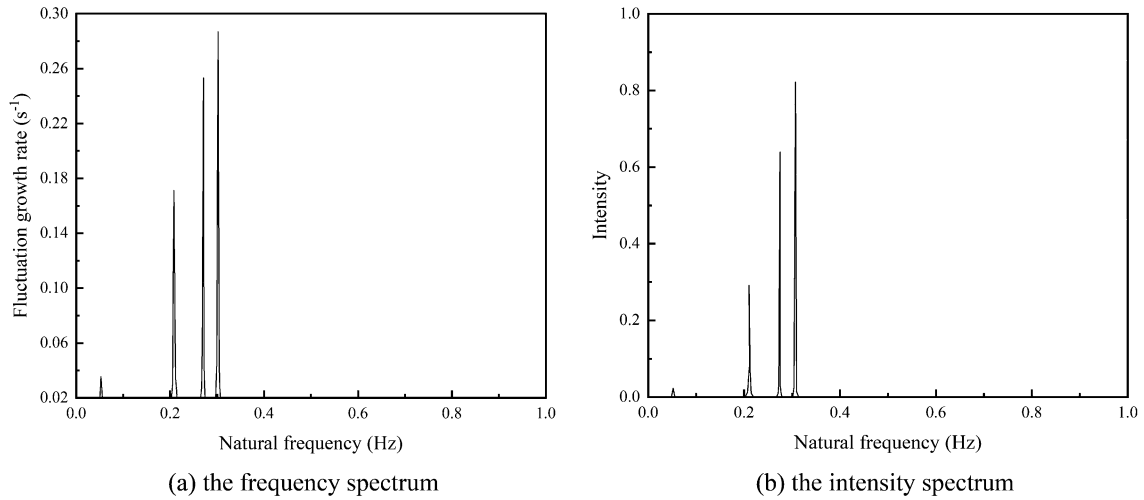
(b) the intensity spectrum

Fig. 2. The frequency and intensity spectrum of the 500-kA cell.

Table I. Mainly contributing modulus analysis of the eigen-frequency of 0.3001–0.2866i

Mode	ω_r	ω_s	Percentage of contribution value
(1, 0)	0	− 0.0408	2.67
(0, 1)	− 0.0972	− 0.0138	7.21
(2, 0)	− 0.0065	− 0.0870	2.98
(1, 1)	− 0.4203	0.1358	45.52
(0, 2)	0.2775	0.1544	26.78
(3, 0)	− 0.0699	− 0.2761	5.32
(2, 1)	0.1918	0.1268	3.64
(1, 2)	0.6988	0	4.36
(0, 3)	− 0.2508	0.0035	1.52

Effect of ACD

The ACD is the distance from the bottom palm of the anode to the top surface of the metal, which not only directly affects the MHD stability but also greatly reduces the electrolysis energy consumption by reducing the distance. Therefore, in order to investigate the influence of ACD on the stability of the electromagnetic field interfacial wave in large-scale cells and obtain the assessment index, the calculation of MHD system stability is applied to a 500-kA cell with ACD of 0.030 m, 0.035 m, 0.040 m, 0.045 m, 0.050 m, 0.055 m, 0.060 m, and 0.070 m, respectively. The other relevant parameters are the same in the electrolysis cell, as described in Table S-

I. A series of aluminum electrolysis frequency spectra are obtained, as shown in Fig. 3a–h.

First, the influence mechanism of ACD is analyzed from a qualitative point of view. Figure 3 is similar to the results of the MHD stability analysis in that the unstable components of the MHD fluctuations are distributed in a low-frequency region. The number of peaks characterizes the number of unstable components of the system, while the height of the peaks reflects the degree of instability of the frequency component. Figure 3 shows that the fluctuation growth rate decreases with increasing ACD, indicating that the MHD stability increases with increasing ACD in large-scale cells.
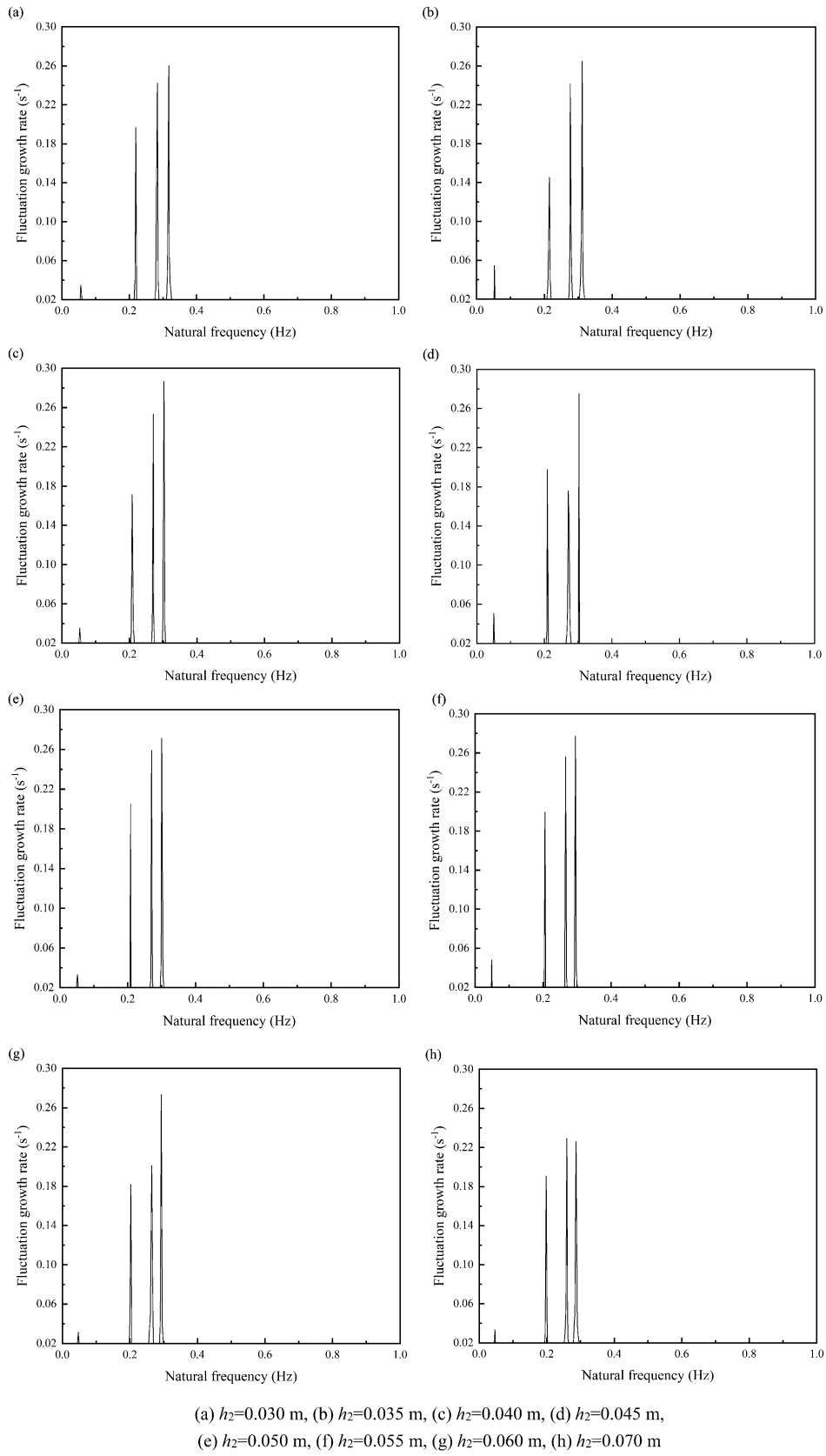
(a) h_2=0.030 m, (b) h_2=0.035 m, (c) h_2=0.040 m, (d) h_2=0.045 m,
(e) h_2=0.050 m, (f) h_2=0.055 m, (g) h_2=0.060 m, (h) h_2=0.070 m

Fig. 3. The frequency and intensity spectra of the 500-kA cell.

Mode Coupling Analysis of Interfacial Stability and Critical Anode–Cathode Distance in a 500-kA Aluminum Electrolysis Cell

2747

Second, the comparison of the changes in the stability of electromagnetic field interfacial wave for each ACD is considered from a quantitative perspective in the aluminum electrolysis cell. In this paper, a modal analysis method and the quantitative index are proposed based on the perspective of mode coupling, combining with the frequency spectra and the results of the modal analysis. Two criteria are proposed to evaluate the stability. The total modulus of the unstable components is used as the assessment index to determine the stability of the electromagnetic field interfacial wave and is defined as:

$$c_1 = |\omega_1 + \omega_2 + \cdots + \omega_n| \qquad (16)$$

where ω is the eigen-frequency and n is the count of the unstable components. ACD is added to the total modulus in the form of a weighting factor as another criterion, which is defined as:

$$c_2 = \frac{|\omega_1 + \omega_2 + \cdots + \omega_n|}{\text{ACD}} \qquad (17)$$

The total modulus is a linear superposition of the instability components corresponding to each low cut-off frequency mode. Figure 3 shows that there are four unstable components under each ACD. The correlation between ACD and stability is investigated by calculating the corresponding total modulus under each ACD using Eqs. 16 and 17.

In order to understand the effects of different ACD on the stability, the ACD zone from 0.035 m to 0.045 m is precisely described by calculating the corresponding total modulus value for every 1-mm increment. Then, the ACD zone from 0.040 m to 0.041 m is subdivided again by calculating the corresponding total modulus value for every 0.2-mm increment. The relationship between ACD and total modulus is presented more clearly through the calculation of each ACD increment. The correlation between the ACD and the total modulus for increments is shown in Fig. 4a.

Figure 4a shows that the total modulus reaches the maximum value of 1.1418 at an ACD of 0.030 m, then, at an ACD of 0.070 m, the minimum value of 1.0199 is reached, which is 10.68% lower than the maximum value within the ACD. Figure 4b demonstrates that the quantitative criterion tends to decrease with increasing ACD, which means that, as the ACD increases, the stability of the aluminum electrolysis cell is improved. In industrial production, raising the anode (increasing the ACD) is used to improve the interfacial wave stability, which verifies that the modal analysis method is consistent with industrial production.

An approximately positive relationship for the stability with ACD can be seen from the data. The ACD is determined not only to avoid a decrease abruptly in the stability of electromagnetic field interfacial wave but also to minimize the energy consumption of the process in the aluminum production, which is a problem worthy of the challenge.

The critical ACD is observed as 0.041 m, whereas, below the critical, the stability decreases abruptly while, above this threshold, the increase of stability is insignificant. The change rate of the total modulus with ACD is the largest, corresponding to the ACD from 0.040 m to 0.041 m shown in Fig. 4a. A minimum total modulus of 1.062 is reached at an ACD of 0.041 m. For the 500-kA cell, the critical value of ACD is 0.041 m. The observed change trend of the critical ACD is consistent with the results of the recent work.

According to the characteristics of the fluid system and the composition model, Bojarevics[19] used the numerical results for the 500-kA test cell (ACD = 0.045 m) to analyze the cell stability under the combination of the effects. Tian[32,33] proposed that the best ACD is 4.2–4.5 cm. Xu[34] established a MHD shallow-water model and concluded the critical ACD for a 300-kA cell is 4.3–4.4 cm. Hua[37] showed that smaller ACD may lead to larger metal pad deformation and more fluctuations of the bath–metal interface. On the premise of maintaining the stability of the electromagnetic field interfacial wave, it meets the lowest energy consumption in the ACD zone of industrial aluminum electrolysis at an ACD of 0.041 m.

Figure 5 shows the eigen-value frequency spectrum of the aluminum electrolysis cell at an ACD of 0.041 m. It can be seen that the eigen-frequency is the unstable component with the largest period and the smallest perturbing frequency, in which the fluctuation growth rate is 0.2100 and the period is 21 s.

The main contributing modulus analysis of the eigen-frequency are shown in supplementary Table S-IV. Similar to the case with the ACD of 0.04 m, the mechanisms of mode coupling, such as (1, 1), (0, 2), are most obvious, accounting for about 70% of the total. The main contributing modulus for the unstable component with the smallest perturbing frequency is at an ACD of 0.041 m, indicating that the unstable component is mainly influenced by the effect of one half-wave in the x-axis, and one half-wave in the y-axis.

The resistivity of the bath and the anode current density of the electrolysis cell is 0.050 Ω cm and 0.80 A/cm^2, respectively. The voltage drops per unit length along with the bath based on the bath composition, electrolysis temperature, and anode current density is calculated as $0.050 \times 0.080 = 0.040$ V/cm. Thus, the voltage drop of the bath at the ACD of 0.041 m is 1.64 V. According to the comprehensive physical field test report of a 500-kA cell by Central South University,[45] the ACD of the cell is 0.042 m and the voltage is 4.0 V. By maintaining the critical ACD of 0.041 m in the electrolysis cell, the voltage can be reduced from 4.0 V to 3.96 V, in which the production

(a) total modulus c_1 as criterion
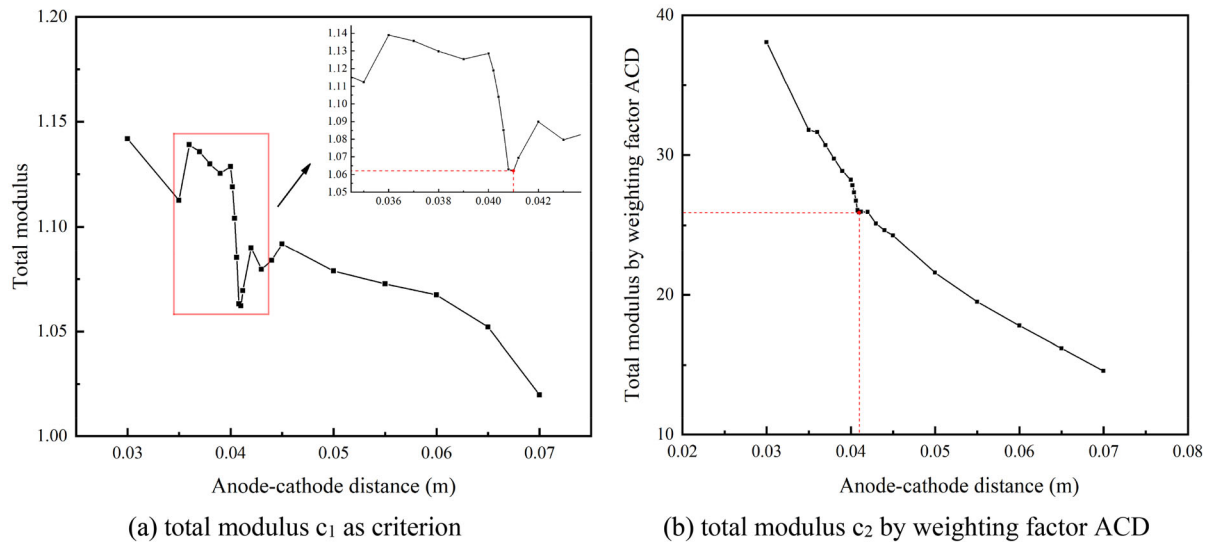

(b) total modulus c_2 by weighting factor ACD

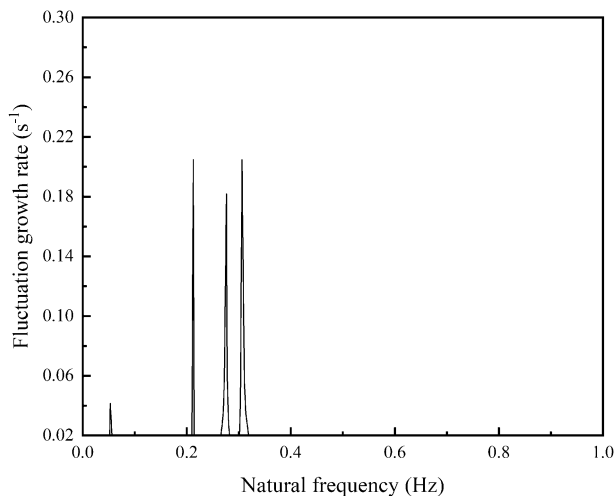Fig. 4. Two criteria to evaluate the stability.

Fig. 5. The frequency spectrum of the 500-kA cell.

process remains stable and the power consumption can be reduced by 120 kWh per ton of aluminum.

The stability of the electromagnetic field interfacial wave can be maintained by raising the anode and increasing the ACD in the industrial production process. However, a higher ACD can also cause the voltage to rise, increasing power consumption. To maintain the stability and reduce the power consumption, it would be more efficient to keep the ACD at 0.041 m. The stability analysis can provide guidance for the MHD design for large-scale aluminum electrolysis cells.

Effect of LWR in Cells

The structural parameters of an aluminum electrolysis cell are important factors that affect the electromagnetic field, flow field distribution, and the stability of the electromagnetic field interfacial wave. Among these, the design of LWR is particularly important compared to other parameters. In this study, in order to investigate the influence of LWR changes on the stability, six sets of 500-kA electrolysis cells with different LWR have been used to calculate the MHD stability. Except for the LWR, all the other parameters of the cells are consistent with those in Table S-I, where the anode–cathode distance is 0.040 m and the aluminum level is 0.20 m. The LWR parameters of each cell are shown in supplementary Table S-V.

The wave spectra of electromagnetic field interfacial stability in aluminum electrolysis cells is shown in Fig. 6a–f. The maximum fluctuation growth rate decreases from 0.3855 s^{-1} to 0.2866 s^{-1}, a decrease of 25.65%. The natural frequency decreases from 0.5 to 0.3 corresponding to the maximum fluctuation growth rate. The maximum fluctuation growth rate and natural frequency of LWR1 to LWR6 tend to decrease with increasing the LWR in the cell, while the electromagnetic field interfacial wave moves towards a more stable trend.

The relationship between the LWR of each cell in Fig. 6a–f and its corresponding stability assessment coefficient is shown in Fig. 7, from which it can be seen that the total moduli of LWR1, LWR3, and LWR6 are 1.47388, 1.3440, and 1.1293, respectively. With increasing the LWR in the cell, the total modulus obviously decreases, and the bath–metal interfacial wave tends to develop in a stable direction, which means that the increasing LWR can effectively enhance the stability of the electromagnetic field interfacial wave in the aluminum cell. The conclusion can be made that it is appropriate to increase the LWR in a limited range. Figure 7 also shows that the LWR changes from 3.6 to 4.5, the change rate of the total modulus value is 0.37. When the LWR is less than 3.6 and greater than 4.5, the change rate of the corresponding total modulus is
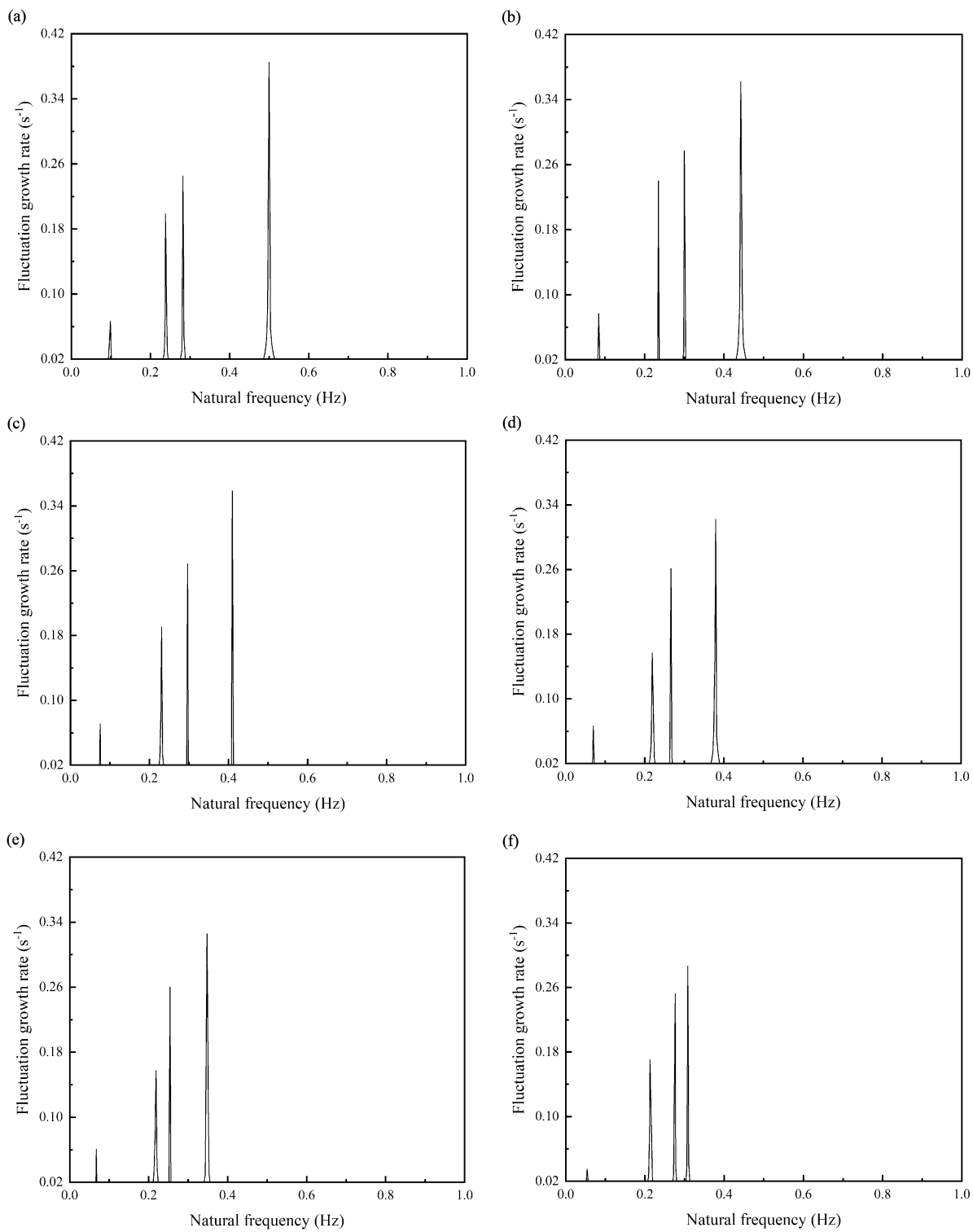
(a) LWR=3.32, (b) LWR=3.66, (c) LWR=4.07,

(d) LWR=4.24, (e) LWR=4.51, (f) LWR=5.37

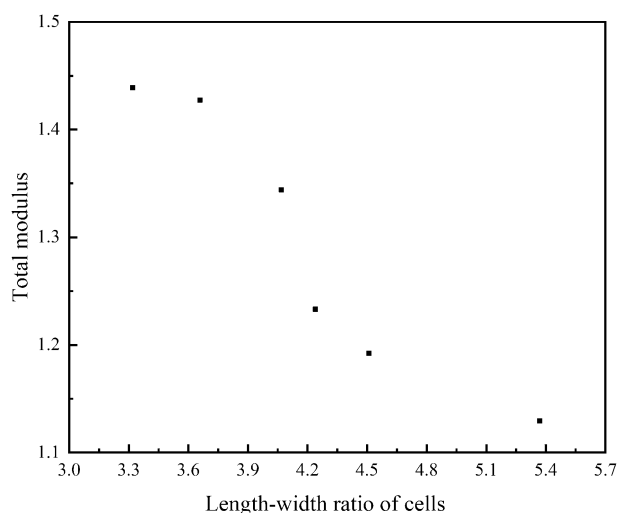Fig. 6. The frequency spectra of aluminum electrolysis cells.

Fig. 7. Correlation between the total modulus and LWR.

0.034 and 0.073, respectively. The change of the LWR has little effect on the stability of the electromagnetic field interfacial wave. The influence of the increasing LWR on the stability is significant when the LWR changes from 3.6 to 4.5. It can provide a theoretical guidance for the design of large-scale aluminum electrolysis cells.

CONCLUSION

A modal analysis method based on the mechanism of mode coupling and the characteristic of total modulus has been proposed to quantitatively describe the stability. The discrete data of the vertical component of the magnetic field were fitted to a continuous function by the least absolute residuals method. The Fourier series method and FEM were used to obtain the eigenvalue equation. The mechanism of each unstable component at different eigen-frequencies were analyzed by custom code in MATLAB. The critical ACD was computed and obtained to improve the stability of certain cell designs. The results are summarized below:

1. Based on theories of electromagnetics and a shallow-water model, the governing equations for describing the bath–metal interfacial wave were established.
2. The frequency spectra and the main contributing moduli of eigen-frequency were obtained by the Fourier series method and FEM. The calculations indicate that there are four unstable frequencies in a 500-kA aluminum electrolysis cell, mainly in the range of 0.05–0.30 Hz. According to quantitative and qualitative analysis, the characteristics of the total modulus are effective for stability assessment.
3. The modal analysis has been investigated with the ACD as the variable. The results show that increasing the ACD is beneficial to improving

the stability of the cell. The critical ACD which can realize the economical and efficient production is 0.041 m.

CONFLICT OF INTEREST

The authors declare that they have no conflict of interest.

SUPPLEMENTARY INFORMATION

The online version contains supplementary material available at https://doi.org/10.1007/s11837-021-04799-4.

REFERENCES

1. A. Gupta and B. Basu, *Trans. Indian Inst. Met.* 72, 2135 (2019).
2. Y. Yang, Y.Q. Guo, W.S. Zhu, and J.B. Huang, *Trans. Nonferrous Met. Soc. China* 29, 1784 (2019).
3. W. Liu, D.F. Zhou, and Z.B. Zhao, *JOM* 71, 2420 (2019).
4. B. Bardet, T. Foetisch, S. Renaudier, J. Rappaz, M. Flueck, and M. Picasso, in *Light Metals 2016* (TMS, Warrendale, 2016), pp 315–319.
5. W. Herreman, C. Nore, J.-L. Guermond, L. Cappanera, N. Weber, and G.M. Horstmann, *J. Fluid Mech.* 122, 598 (2019).
6. T. Sele, *Metall. Trans. B* 8, 613 (1977).
7. N. Urata, K. Mori, and H. Ikeuchi, *J. Jpn. Inst. Light Met.* 26, 573 (1976).
8. N. Urata, in *Light Metals 1985* (TMS, Warrendale, 1985), pp 581–591.
9. A.D. Sneyd, *J. Fluid Mech.* 156, 223 (1985).
10. P.A. Davidson, and R.I. Lindsay, in *Light Metals 1997* (TMS, Warrendale, 1997), pp 437–442.
11. O. Zikanov, A. Thess, P.A. Davidson, and D.P. Ziegler, *Metall. Mater. Trans. B* 31, 1541 (2000).
12. T. Weyens, J.M. Reynolds-Barredo, and A. Loarte, *Comput. Phys. Commun.* 242, 60 (2019).
13. J.L. Ding, J. Li, H.L. Zhang, Y.J. Xu, S. Yang, and Y.X. Liu, *Cent. South Univ.* 21, 4097 (2014).
14. M. Dupuis and M. Page, in *Light Metals 2016* (TMS, Warrendale, 2016), pp 909–914.
15. M. Dupuis and M. Page, in *Light Metals 2016* (TMS, Warrendale, 2016), pp 58–62.
16. V. Bojarevics and M. Romerio, *Eur. J. Mech. B* 13, 33 (1994).
17. V. Bojarevics and S. Sira, in *Light Metals 2014* (TMS, Warrendale, 2014), pp 685–690.
18. V. Bojarevics and K. Pericleous, in *Light Metals 2006* (TMS, Warrendale, 2006), pp 347–352.
19. V. Bojarevics, in *Light Metals 2013* (TMS, TMS, Warrendale, 2013), pp 609–614.

20. V. Bojarevics and A. Tucs, in *Light Metals 2017* (TMS, Warrendale, 2013), pp 677–686.
21. V. Bojarevics and M. Dupuis, in *Light Metals 2021* (TMS, Warrendale, 2021), pp 565–571.
22. M. Dupuis and V. Bojarevics, in *Light Metals 2020* (TMS, Warrendale, 2020), pp 495–509.
23. H.J. Sun, O. Zikanov, and D.P. Ziegler, *Fluid Dyn. Res.* 35, 255 (2004).
24. M. Kadkhodabeigi and Y. Saboohi, in *Light Metals 2007* (TMS, Warrendale, 2007), pp 345–351.
25. S. Molokov, G. El, and A. Lukyanov, *Theor. Comput. Fluid Dyn.* 122, 6 (2019).
26. S. Molokov, *Europhys. Lett.* 121, 44001 (2018).
27. A. Pedcenko, S. Molokov, and B. Bardet, *Metall. Mater. Trans. B* 48, 6 (2017).
28. S.Y. Ruan, F.Y. Van, M. Dupuis, V. Bojarevics, and J.F. Zhou, in *Light Metals 2013* (TMS, Warrendale, 2013), pp 603–607.
29. Y. Yang, S.H. Yao, and X.B. Yi, in *Light Metals 2014* (TMS, Warrendale, 2014), pp 703–708.
30. B.K. Li, F. Wang, X.B. Zhang, F.S. Qi, and N.X. Feng, in *AIP Conference Proceedings* (American Institute of Physics, Melville, 2012), pp 865–868.
31. Q. Wang, B.K. Li, F. Wang, and N.X. Feng, in *Light Metals 2013* (TMS, Warrendale, 2013), pp 615–619.
32. Y.F. Tian, *Nonferrous Met.* 25, 23 (2009).
33. Y.F. Tian, *Light Met.* 2, 31 (2011).
34. Y.J. Xu, J. Li, H.L. Zhang, and Y.Q. Lai, *Chin. J. Nonferrous Met.* 21, 191 (2011).
35. H.L. Zhang, J. Li, Z.G. Wang, Y.J. Xu, and Y.Q. Lai, *JOM* 62, 26 (2010).
36. X.J. Lu, H.X. Zhang, Z.X. Han, K.J. Wang, C.H. Guan, Q.D. Sun, W.W. Wang, and M.R. Wei, *Trans. Nonferrous Met. Soc. China* 30, 1124 (2020).
37. J.S. Hua, M. Rudshaug, C. Droste, and R. Jorgensen, *Metall. Mater. Trans. B* 49, 1246 (2018).
38. A. Tucs, V. Bojarevics, and K. Pericleous, *J. Fluid Mech.* 852, 453 (2018).
39. A. Tucs, V. Bojarevics, and K. Pericleous, *Europhys. Lett.* 124, 24001 (2018).
40. N. Weber, P. Beckstein, W. Herreman, G.M. Horstmann, C. Nore, F. Stefani, and T. Weier, *Phys. Fluids* 29, 54101 (2017).
41. G.M. Horstmann, N. Weber, and T. Weier, *J. Fluid Mech.* 845, 1 (2018).
42. O. Zikanov, *Theor. Comput. Fluid Dyn.* 32, 325 (2018).
43. M. Segatz and C. Droste, in *EMC 2001: European Metallurgical Conference* (GDMB, Clausthal-Zellerfeld, 2001), pp. 117–128.
44. N. Urata, in *Light Metals 2005* (TMS, Warrendale, 2005), pp 455–460.
45. H.S. Li, W.Y. Hou, and Q.H. Li (Central South University, Changsha, 2019).